On the incorporation of the geometric phase in general single potential energy surface dynamics: A removable approximation to ab initio data

Christopher L. Malbon, Xiaolei Zhu, Hua Guo, and David R. Yarkony

Citation: The Journal of Chemical Physics **145**, 234111 (2016); doi: 10.1063/1.4971369

View online: https://doi.org/10.1063/1.4971369

View Table of Contents: http://aip.scitation.org/toc/jcp/145/23

Published by the American Institute of Physics

Articles you may be interested in

Dynamic mapping of conical intersection seams: A general method for incorporating the geometric phase in adiabatic dynamics in polyatomic systems
The Journal of Chemical Physics **147**, 044109 (2017); 10.1063/1.4990002

Multistate, multichannel coupled diabatic state representations of adiabatic states coupled by conical intersections. CH_2OH photodissociation
The Journal of Chemical Physics **146**, 134302 (2017); 10.1063/1.4978708

Perspective: Computing (ro-)vibrational spectra of molecules with more than four atoms
The Journal of Chemical Physics **146**, 120902 (2017); 10.1063/1.4979117

High order path integrals made easy
The Journal of Chemical Physics **145**, 234103 (2016); 10.1063/1.4971438

Full-dimensional ground- and excited-state potential energy surfaces and state couplings for photodissociation of thioanisole
The Journal of Chemical Physics **146**, 064301 (2017); 10.1063/1.4975121

Practical approximation of the non-adiabatic coupling terms for same-symmetry interstate crossings by using adiabatic potential energies only
The Journal of Chemical Physics **146**, 064107 (2017); 10.1063/1.4975323

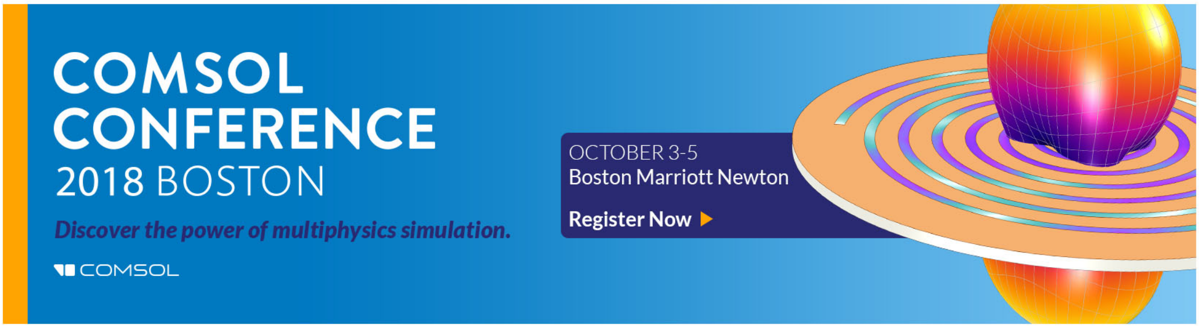

COMSOL CONFERENCE
2018 BOSTON
Discover the power of multiphysics simulation.
COMSOL
OCTOBER 3-5
Boston Marriott Newton
Register Now

THE JOURNAL OF CHEMICAL PHYSICS **145**, 234111 (2016)

On the incorporation of the geometric phase in general single potential energy surface dynamics: A removable approximation to *ab initio* data

Christopher L. Malbon,[1] Xiaolei Zhu,[2] Hua Guo,[3] and David R. Yarkony[1]
[1]*Department of Chemistry, Johns Hopkins University, Baltimore, Maryland 21218, USA*
[2]*Department of Chemistry, Stanford University, Stanford, California 94305, USA*
[3]*Department of Chemistry and Chemical Biology, University of New Mexico, Albuquerque, New Mexico 87131, USA*

(Received 4 October 2016; accepted 18 November 2016; published online 20 December 2016)

For two electronic states coupled by conical intersections, the line integral of the derivative coupling can be used to construct a complex-valued multiplicative phase factor that makes the real-valued adiabatic electronic wave function single-valued, provided that the curl of the derivative coupling is zero. Unfortunately for *ab initio* determined wave functions, the curl is never rigorously zero. However, when the wave functions are determined from a coupled two diabatic state Hamiltonian $\mathbf{H}^d$ (fit to *ab initio* data), the resulting derivative couplings are by construction curl free, except at points of conical intersection. In this work we focus on a recently introduced diabatization scheme that produces the $\mathbf{H}^d$ by fitting *ab initio* determined energies, energy gradients, and derivative couplings to the corresponding $\mathbf{H}^d$ determined quantities in a least squares sense, producing a removable approximation to the *ab initio* determined derivative coupling. This approach and related numerical issues associated with the nonremovable *ab initio* derivative couplings are illustrated using a full 33-dimensional representation of phenol photodissociation. The use of this approach to provide a general framework for treating the molecular Aharonov Bohm effect is demonstrated. *Published by AIP Publishing.* [http://dx.doi.org/10.1063/1.4971369]

I. INTRODUCTION

Conical intersections are understood to be the engines of nonadiabatic radiationless transitions as they efficiently move wave packets between potential energy surfaces (PESs).[1–7] A signature property of conical intersections is the geometric phase.[8–11] The geometric phase, also known as the Berry phase,[11] refers to the sign change incurred by a real-valued adiabatic electronic wave function transported around a closed loop containing a conical intersection. While the geometric phase effect is well-documented in (two state) Jahn-Teller systems,[12] and specialized techniques exist for determining the relevant PESs in the frequently studied X_3 systems,[13] much less attention has been paid to a more insidious occurrence of the geometric phase effect, a single adiabatic PES manifestation known as the Molecular Aharonov Bohm (MAB) effect, discovered by Mead and Truhlar[10,14] over 35 years ago. In their classic analysis of this subtle combination of topographical and dynamical factors, energetic considerations restrict nuclear motion to a single Born-Oppenheimer PES, but the usual implementation of Born-Oppenheimer dynamics using real-valued electronic states and single-valued nuclear wave functions is flawed owing to the existence of energetically inaccessible points of conical intersection whose dynamical relevance is attributable to, as originally formulated, energetically accessible paths[10,14] or more recently quantum mechanical tunneling[15,16] paths surrounding those points. The MAB effect is then a quantum effect arising from interference among "trajectories" following the different paths around the energetically inaccessible conical intersection.[10,14,17,18]

The archetypical example of the MAB effect is the reaction of $H_2 + H$ on the ground state PES at total energies less than that of the minimum energy conical intersection at approximately 2.75 eV relative to H + H_2.[19] It has been treated by several groups over the last quarter century.[20–30] In this system, the MAB effect is small and only recently has it been suggested that it could be seen under ultra-cold conditions.[31,32]

Other opportunities for observing the MAB effect exist and are of more practical concern. Photochemistry is an area where the MAB effect can be of great importance.[33] Recent model calculations have clearly demonstrated that the inclusion of the geometric phase has a decisive influence on the tunneling lifetimes of photo-generated metastable states.[15,34] Like the reactive scattering case mentioned above, the interference attributed to the geometric phase for trajectories passing around the conical intersection retards the delocalization or dissociation of a quantum state.

Recently, there has been a renewed interest in how this manifestation of the geometric phase impacts nuclear motion in the adiabatic representation in the vicinity of a conical intersection.[34–39] These recent studies[18,26,28,40,41] account for the geometric phase using variants of the vector potential approach introduced by Mead and Truhlar[10,14] to treat the MAB effect. The key formal challenge in using this vector potential approach, and hence in treating the MAB effect, is the determination of the complex-valued phase factor, $\exp(iA)$, and associated vector potential, $i\nabla A$, to be included in the adiabatic Hamiltonian to account for the geometric phase. The phase factor $\exp(iA)$ in turn reflects the locus of points on the conical intersection seam and the description of paths that surround such points. Apart from two-dimensional model systems in which the diabatic and adiabatic representations can be uniquely defined,[34,38,39] the majority of past theoretical studies, explicitly including the geometric phase, have been restricted to X_3 systems. These systems have the advantage that the conical intersection seam is determined by symmetry and the requisite closed loop containing the intersection is given in hyperspherical coordinates by the hyperangle.[20] For systems without high symmetry, such as HO_2 for which the conical intersections are either in linear or C_{2v} geometries, the vector potential has been derived from a model (diatom-in-molecule) Hamiltonian.[42]

In this work, we consider the general case, untreated thus far, where the symmetry cannot be used to determine either the conical intersection seam or the closed loops that contain it. Our approach is to derive the explicit expression for the vector potential directly from a diabatic Hamiltonian, $\mathbf{H}^d$, fit to the *ab initio* data.[43] In Section II, the well-known mathematics behind the MAB effect is reviewed in order to make clear the numerical results presented in Section III. Section IV summarizes and describes directions for future work.

II. THE SINGLE POTENTIAL ENERGY SURFACE GEOMETRIC PHASE (MAB) EFFECT

A. Definitions

In the adiabatic Born-Oppenheimer approximation, the total wave function ($\Psi^T_{J,k}$) is written as

$$\Psi^T_{J,k}(\mathbf{q},\mathbf{R}) = \Psi^{(a)}_J(\mathbf{q};\mathbf{R})\chi^k_J(\mathbf{R}), \tag{1}$$

where the adiabatic states $\Psi^{(a)}_J(\mathbf{q};\mathbf{R})$ satisfy the electronic Schrödinger equation

$$[H^e(\mathbf{R}) - E^{(a),J}(\mathbf{R})]\Psi^{(a)}_J(\mathbf{q};\mathbf{R}) = 0, \tag{2}$$

where (a) denotes adiabatic, $\mathbf{q}$ denotes the coordinates of $3N^{el}$ electrons, and $\mathbf{R}$ denotes $3N^{atom}$ the nuclear coordinates. There are two sources of $\Psi^{(a)}_J(\mathbf{q};\mathbf{R})$. One is *ab initio* (*ab*) adiabatic wave functions $\Psi^{(a),(ab)}_J(\mathbf{q};\mathbf{R})$, which for concreteness, although it is certainly not a necessity, we take to be expanded in a configuration state function (*CSF*) basis $\psi_\alpha(\mathbf{q};\mathbf{R})$, $\alpha = 1,\ldots,N^{CSF}$ basis,

$$\Psi^{(a),(ab)}_J(\mathbf{q};\mathbf{R}) = \sum_{\alpha=1}^{N^{CSF}} c^J_\alpha(\mathbf{R})\psi_\alpha(\mathbf{q};\mathbf{R}), \tag{3a}$$

where the $\mathbf{c}^J$ satisfy

$$[\mathbf{H}^{CSF}(\mathbf{R}) - \mathbf{I}E^{(a),(ab),J}(\mathbf{R})]\mathbf{c}^J(\mathbf{R}) = 0. \tag{3b}$$

The other is model wave functions,

$$\Psi^{(a),(m)}_J(\mathbf{q};\mathbf{R}) = \sum_{\alpha=1}^{N^{state}} d^J_\alpha(\mathbf{R})\Psi^{(d)}_\alpha(\mathbf{q};\mathbf{R}), \tag{4a}$$

which satisfy the electronic Schrödinger equation

$$[\mathbf{H}^d(\mathbf{R}) - \mathbf{I}E^{(a),(m),J}(\mathbf{R})]\mathbf{d}^J(\mathbf{R}) = 0, \tag{4b}$$

where $\mathbf{H}^d$ is the coupled diabatic state Hamiltonian fit to the coupled adiabatic states of interest and (m) stands for model (see the Appendix).

The nuclear wavefunction $\chi^k_J(\mathbf{R})$ satisfies the adiabatic nuclear Schrödinger equation

$$[H^{ad} - E^T_k]\chi^k_K(\mathbf{R}) = 0, \tag{5a}$$

where *ad* stands for adiabatic and H^{ad} (with $\hbar = 1$ hereafter) is given by

$$H^{ad}(\mathbf{R}) = \sum_{n=1}^{N^{atom}} \frac{1}{2M_n}(-i\nabla_n)^2 + k^{K,K}(\mathbf{R}) + E^{(a),K}(\mathbf{R}), \tag{5b}$$

where $\nabla_n = (\frac{\partial}{\partial R_{n,x}}, \frac{\partial}{\partial R_{n,y}}, \frac{\partial}{\partial R_{n,z}})$ and

$$k^{K,K}(R) = \sum_{n=1}^{N^{atom}} k^{K,K}_{n,n}(\mathbf{R})/(2M_n), \tag{6a}$$

where

$$k^{K,K}_{n,n} = \left\langle \nabla_n\Psi^{(a)}_K(\mathbf{q};\mathbf{R})\right| \cdot \left.\nabla_n\Psi^{(a)}_K(\mathbf{q};\mathbf{R})\right\rangle_{\mathbf{q}} \tag{6b}$$

$$= \sum_L \mathbf{f}^{(a),L,K}_n(\mathbf{R}) \cdot \mathbf{f}^{(a),L,K}_n(\mathbf{R}) \tag{6b$'$}$$

and

$$\mathbf{f}^{(a),L,K}_n(\mathbf{R}) = \left\langle \Psi^{(a)}_L(\mathbf{q};\mathbf{R})\right|\nabla_n\left.\Psi^{(a)}_K(\mathbf{q};\mathbf{R})\right\rangle_{\mathbf{q}} \tag{6c}$$

are the Diagonal Born-Oppenheimer Correction (DBOC)[44–49] and derivative coupling, respectively. In Eq. (6b′), the sum on L runs over all states. The DBOC in Eq. (6b) can be evaluated using analytical gradient techniques.[47,48] In this work, we will use Eq. (6b′) with L truncated.

Provided that $\chi^k_K(\mathbf{R})$ is single-valued, as is most convenient, Ψ^T_k is double-valued if conical intersections of states K and $K + 1$ exist. This is untenable, so Eq. (1) is multiplied by a complex valued phase factor, $\exp[iA_K(\mathbf{R})]$, whose sole purpose is to make $\Psi^{(a)}_K(\mathbf{q};\mathbf{R})$ single-valued.[10,14] The principal formal challenge in this work is the determination of $A_K(\mathbf{R})$. This quantity is readily defined in two-dimensional models as the mixing angle between the adiabatic and diabatic states,[10,34] or using the polar angle with the single point of conical intersection located at the origin of a polar coordinate system. However, it is much more difficult to do so for a general molecular system. Here, we propose a way to determine this quantity based on *ab initio* computed derivative couplings. There are several ways to get to the final result. Here, we use an approach emphasizing the connection to the geometric phase effect.

B. The MAB Hamiltonian

We begin by describing the vicinity of an arbitrary conical intersection at $\mathbf{R}^{ci}$ between states I and J. This discussion (through Eq. (11b)) is excerpted from Ref. 50. In the vicinity of $\mathbf{R}^{ci}$ the electronic Schrödinger equation in the electronic basis $(\Psi^{(a),(ab)}_I(\mathbf{q};\mathbf{R}^{ci}), \Psi^{(a),(ab)}_J(\mathbf{q};\mathbf{R}^{ci}))$ and using orthogonal intersection adapted coordinates[51] (x,y,z_i; $1 \le i \le 3N^{atom}-2$) is given by

$$(\mathbf{H}^{ci}(\mathbf{R}) - \mathbf{I}E^{(a),(ci)}_{\pm}(\mathbf{R}))\zeta^{(a),(ci),\pm}(\mathbf{R}) = 0. \tag{7a}$$

Here $\mathbf{R} = \mathbf{R}^{ci} + \delta\mathbf{R}$,

$$\mathbf{H}^{ci}(\mathbf{R}) = S(\mathbf{R})\mathbf{I} + gx\begin{pmatrix}1 & 0\\ 0 & -1\end{pmatrix} + hy\begin{pmatrix}0 & 1\\ 1 & 0\end{pmatrix}, \tag{7b}$$

(ci) stands for conical intersection,

$$\mathbf{h}^{I,J}(\mathbf{R}) = \mathbf{c}^{I}(\mathbf{R}^{ci})^{\dagger}\nabla_{\mathbf{R}}\mathbf{H}^{CSF}(\mathbf{R})\mathbf{c}^{J}(\mathbf{R}^{ci}), \tag{8a}$$

$$2\,\mathbf{g}^{I,J}(\mathbf{R}) = \mathbf{h}^{J,J}(\mathbf{R}) - \mathbf{h}^{I,I}(\mathbf{R}), \tag{8b}$$

$$S(\mathbf{R}) = \mathbf{s}(\mathbf{R})\cdot\delta\mathbf{R} = s_x x + s_y y + \sum_{i=1}^{3N^{atom}-2} s_{z_i} z_i, \tag{8c}$$

where $g = \|\mathbf{g}^{I,J}\|$, $h = \|\mathbf{h}^{I,J}\|$, $\mathbf{s} = (\mathbf{h}^{I,I} + \mathbf{h}^{J,J})/2$, $s_x = \mathbf{s}(\mathbf{R})\cdot\hat{\mathbf{x}}$, $s_y = \mathbf{s}(\mathbf{R})\cdot\hat{\mathbf{y}}$, and $s_{z_i} = \mathbf{s}(\mathbf{R})\cdot\hat{\mathbf{z}}_i$. In orthogonal intersection adapted coordinates, the x-axis is parallel to $\mathbf{g}^{I,J}$, the y-axis is parallel to $\mathbf{h}^{I,J}$; the $\mathbf{z}_i$ are mutually orthogonal and orthogonal to the (x,y) plane, which is the usual g-h plane. Then, for cylindrical polar coordinates with $(x, y) = (\rho\cos\theta, \rho\sin\theta)$, and suppressing the remaining (z_i) coordinates

$$\begin{aligned}\Psi_I^{(a),(w)}(\mathbf{R}) &\xrightarrow[\rho\to 0]{} \zeta^{(a),(ci),-}(\rho,\theta)\\ \Psi_J^{(a),(w)}(\mathbf{R}) &\xrightarrow[\rho\to 0]{} \zeta^{(a),(ci),+}(\rho,\theta),\end{aligned} \tag{9}$$

for $(w) = (ab)$ and (m), we readily derive two results[50]

$$\zeta^{(a),(ci),\pm}(\rho,\theta+2\pi) = -\zeta^{(a),(ci),\pm}(\rho,\theta) \tag{10a}$$

and

$$\oint \mathbf{f}^{(a),(ci),+,-}(\mathbf{R}')\cdot d\mathbf{R}' = \pi. \tag{10b}$$

Eq. (10a) is the geometric phase. Eq. (10b) follows from[50]

$$\left\langle \zeta^{(a),(ci),-}\left|\frac{\partial}{\partial\theta}\zeta^{(a),(ci),+}\right.\right\rangle = \frac{1}{2}\frac{gh}{(g\cos\theta)^2 + (h\sin\theta)^2}, \tag{11a}$$

which is independent of ρ and

$$\left\langle \zeta^{(a),(ci),-}\ \left|\frac{\partial}{\partial\rho}\ \zeta^{(a),(ci),+}\right.\right\rangle = 0, \tag{11b}$$

obtained from the solutions to Eqs. (7a) and (7b). Since Eqs. (10a) and (10b) are derived from Eqs. (7a) and (7b), ρ is required to be infinitesimal. In the second equality, $\oint$ denotes the circulation, the line integral along a circle of radius r. If either of the linear terms is removed from Eq. (7b) (so that the lowest order term is quadratic), the intersection is not a conical intersection and we find

$$\zeta^{(a),(nci),\pm}(\rho,\theta+2\pi) = \zeta^{(a),(nci),\pm}(\rho,\theta) \tag{12a}$$

and

$$\oint \mathbf{f}^{(a),(nci),+,-}(\mathbf{R}')\cdot d\mathbf{R}' = 0, \tag{12b}$$

that is, no geometric phase. Eqs. (10a) and (10b) establish the key correspondence between the geometric phase and the circulation of the derivative coupling.

Since $e^{i\pi} = -1$, defining the phase factor as the exponential of a line integral

$$\exp[iA_K(\mathbf{R})] = \exp\Big(i\int_{\mathbf{R}^0}^{\mathbf{R}} \mathbf{f}^{(a),(w),I,J}(\mathbf{R}')\cdot d\mathbf{R}'\Big) \tag{13a}$$

from Eqs. (10b) and (12b) we find that the product of the electronic wave function and the phase factor is single-valued, that is,

$$\begin{aligned}&\Psi_K^{(a),(w)}(\rho,\theta+2\pi)\exp[iA_K(\rho,\theta+2\pi)]\\ &\quad= \exp[iA_K(\rho,\theta)]\Psi_K^{(a),(w)}(\rho,\theta)\end{aligned} \tag{13b}$$

for $K = I$ or J and $(w) = (ab)$, (m) precisely as required. However, in Eq. (13b) ρ is required to be infinitesimal. For Eq. (13a) to be useful, the line integral in that equation must vanish for all closed paths provided the closed path does not contain a singularity, i.e., a conical intersection.

We now explain how this criterion is related to the idea of removable and nonremovable derivative couplings introduced by Mead and Truhlar.[52] From the two adiabatic state derivative coupling using a nominally diabatic basis, that is a basis for which $\mathbf{f}_{\alpha}^{(d),(w),L,K}(\mathbf{R}) = 0$, and starting with the inverse of the adiabatic to diabatic state (AtD) transformation

$$\begin{pmatrix}\Psi_I^{(a),(w)}\\ \Psi_J^{(a),(w)}\end{pmatrix} = \begin{pmatrix}\cos\Theta(\mathbf{R}) & \sin\Theta(\mathbf{R})\\ -\sin\Theta(\mathbf{R}) & \cos\Theta(\mathbf{R})\end{pmatrix}\begin{pmatrix}\Psi_s^{(d),(w)}\\ \Psi_t^{(d),(w)}\end{pmatrix}, \tag{14}$$

we obtain

$$\nabla\Theta(\mathbf{R}) = -\mathbf{f}^{(a),(w),I,J}(\mathbf{R}), \tag{15}$$

for $(w) = (ab)$ or (m). For $(w) = (ab)$; Eq. (15) is used to define $\Theta(\mathbf{R})$. Mead and Truhlar[52] using the curl condition[53] showed that Eq. (15) only has a solution if the adiabatic and diabatic spaces have the same dimension. Since $N^{CSF} >> 2$, $\mathbf{f}^{(a),(ab),I,J}(\mathbf{R})$ has a curl and Eq. (15) has no solution. This derivative coupling is referred to as nonremovable[52] since it cannot be eliminated (removed) by the AtD transformation, the inverse of Eq. (14). For diabatized representations, $(w) = (m)$, see Eq. (4), the situation is different. $\Theta(\mathbf{R})$ is *defined* by the diabatization procedure and Eq. (15) is used to compute the derivative coupling $\mathbf{f}^{(a),(m),I,J}(\mathbf{R})$ in a representation assumed diabatic. Then, from Eq. (15) in the two-state case $\mathbf{f}^{(a),(m),I,J}(\mathbf{R})$ is by construction the gradient of a scalar and consequently has no curl. The derivative coupling $\mathbf{f}^{(a),(m),I,J}(\mathbf{R})$ defined in this way is termed removable[52] since the AtD transformation eliminates (removes) it. Thus Eq. (15) is only valid for (w) = (m). From an alternative perspective, $\mathbf{f}^{(a),(m),I,J}(\mathbf{R})$ is a removable approximation to the nonremovable $\mathbf{f}^{(a),(ab),I,J}(\mathbf{R})$.

Using Eq. (15) and the following result from vector calculus concerning line integrals, we demonstrate the path independence of the line integral in Eq. (13a). The line integral of Eq. (15) gives

$$\int_{\mathbf{R}^0}^{\mathbf{R}}\left[\sum_{i=1}^{3N^{atom}} \mathbf{f}_i^{(a),(w),I,J}(\mathbf{R}')\cdot \mathbf{dR}_i'\right] = \int_{\mathbf{R}^0}^{\mathbf{R}}\left[\sum_{i=1}^{3N^{atom}} \nabla_i\Theta(\mathbf{R}')\cdot \mathbf{dR}_i'\right]. \tag{16a}$$

Using t to parametrize the path, this becomes

$$\begin{aligned}&= \int_{\mathbf{R}^0}^{\mathbf{R}}\left[\sum_{i=1}^{3N^{atom}} \nabla_i\Theta(\mathbf{R}')\cdot\frac{\partial\mathbf{R}_i'}{\partial t}\right]dt = \int_0^t \frac{d}{dt}\Theta(\mathbf{R}(t))dt\\ &\qquad\qquad = \Theta(\mathbf{R}(t)) - \Theta(\mathbf{R}(0)).\end{aligned} \tag{16b}$$

Thus, if Θ satisfies Eq. (15), then it is a state function and it depends only on its end points, not its path. The converse is also true. Thus, $\exp(i\int_{\mathbf{R}^0}^{\mathbf{R}}\mathbf{f}^{(a),(w),I,J}(\mathbf{R}')\cdot d\mathbf{R}')$, Eq. (13a) is path independent if and only if the derivative coupling is removable. Here the singularities have been removed. The contributions from the singularities (conical intersections) are given by Eq. (10b). These observations are demonstrated numerically in Section III.

The diabatization procedure used to determine $\Theta(\mathbf{R})$ is a key issue. For a diabatization to be useable, it must generate the singularities in $\mathbf{f}^{(a),(m),I,J}(\mathbf{R})$ at points of conical intersection and only at points of conical intersection. Diabatizations tend to get the conical intersections singularities correct. However, the defining equations of some classes of diabatizations necessarily introduce fallacious or spurious singularities on subspaces of the same dimension as that of the true conical intersections. The diabatization used in this work, described in the Appendix, does not suffer from this limitation, and makes $\mathbf{f}^{(a),(m),I,J}(\mathbf{R})\sim\mathbf{f}^{(a),(ab),I,J}(\mathbf{R})$ in a least squares sense.[43] The complete description of this potential limitation is beyond the scope of this work, but such a description can be found in two recent publications.[54,55]

There are other ways to derive Eq. (13a). One general method involves the topological matrix introduced by Baer.[56–58] It should also be pointed out that the line integral in Eq. (13a) picks up all the singular conical intersections contained in a loop.

With the phase factor given by Eq. (13a), the single-state nuclear Schrödinger equation in the adiabatic representation becomes[59,60]

$$[H^{MAB}-E_k^T]\chi_I^k(\mathbf{R})=\mathbf{0}, \tag{17a}$$

where

$$H^{MAB}=\sum_{n=1}^{N^{atom}}\frac{1}{2M_n}(-i\nabla_n+\mathbf{f}_n^{(a),(m),I,J})^2+k^{I,I}(\mathbf{R})+E_I^{(a),(m)}(\mathbf{R}), \tag{17b}$$

and the DBOC is approximated by

$$k^{I,I}(\mathbf{R})\approx\sum_{n=1}^{N^{atom}}\frac{1}{2M_n}\mathbf{f}_n^{(a),(m),I,J}(\mathbf{R})\cdot\mathbf{f}_n^{(a),(m),I,J}(\mathbf{R}). \tag{17c}$$

The approximation for the DBOC used in Eq. (17c) captures precisely its singular character as the conical intersection is approached. The singularity causes the nuclear wave function to vanish at the conical intersection.[61–63]

Eqs. (17a)–(17c) are key results of this work providing a general method of incorporating the MAB effect into single potential energy surface dynamics. Because of its position in the parentheses in Eq. (17b), $\mathbf{f}^{(a),(m),I,J}$ is denoted as a vector potential. The caveat here is the need to use a fit surface approximation to the *ab initio* determined coupled potential energy surfaces since that is used to determine the removable approximation to the derivative coupling. This should not be considered a significant limitation, if a limitation at all, since in general fit surfaces are preferred for detailed quantum mechanical computations. This preference is a consequence of the fact that since our fitting procedure fits the energies (and energy gradients and derivative couplings) in a least squares sense, it can smooth out discontinuities attributable to orbitals entering and leaving the active space, a problem endemic to multireference calculations which are essential for the description of nonadiabatic processes. In this sense the fit coupled potential energy surfaces are a better representation of the true coupled potential energy surfaces than the *ab initio* data from which they are derived. See Ref. 43 for an example of this smoothing.

TABLE I. Energies (in cm^{-1}) of key extrema and g, h, s_x in a.u. at mex(S_1-S_2).

	$\mathbf{H}^{d,(4)}$	$\mathbf{H}^{d,(2)}$
min(S_1)	37 577	37 543
ts(S_1)	43 426	43 619
mex(S_1-S_2)	44 280	44 287
g	0.137 98	0.137 11
h	0.013 77	0.013 99
s_x	−0.073 93	−0.081 48

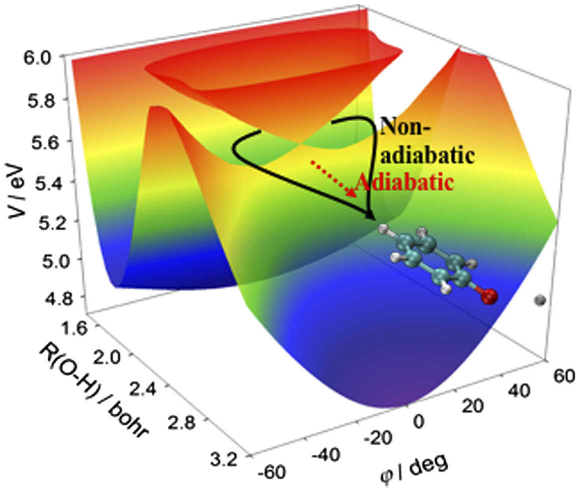

FIG. 1. S_1 and S_2 PESs and their conical intersection for phenol photodissociation, $C_6H_5OH + h\nu \rightarrow C_6H_5O + H$. Reprinted with permission from H. Guo and D. R. Yarkony, Phys. Chem. Chem. Phys. **18**, 26335 (2016). Copyright 2016 PCCP Owner Societies.

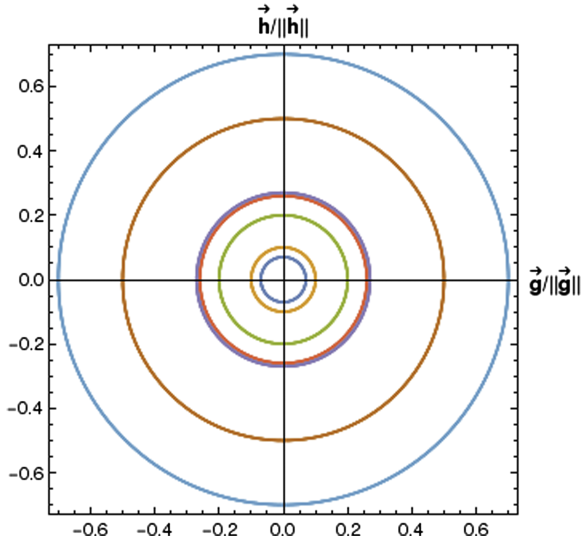

FIG. 2. Loops used to evaluate $C(w,(0,0,0),r)$, $w = 2,4$, in Figures 3 and 4.

The use of line integrals of the derivative coupling was reported in curl-free circumstances by Baer.[53] Attempts to use this approach with derivative couplings obtained directly from *ab initio* calculations, $\mathbf{f}^{(a),(ab),I,J}(\mathbf{R})$, were justifiably criticized[57,64] as being path dependent. The availability of both the *ab initio* (nonremovable) derivative coupling and a removable approximation based on reliable coupled potential energy surfaces may permit numerical studies of this approximation.

C. Implications for nuclear dynamics

In quantum dynamics on a single potential energy surface, the geometric phase can be introduced by a complex-valued phase [Eq. (13a)], which leads to additional terms that involve both vectorial (∇) and scalar terms, the DBOC.[10,26,29,42] The $A_K(\mathbf{R})$ in the phase factor is an explicit function of the nuclear coordinates, and thus diagonal in a grid representation. It commutes with the potential energy operator and the DBOC, and as a result its introduction into the Hamiltonian only modifies the kinetic energy operator. In principle, these additional terms can be accurately represented in the discrete variable representation and its corresponding finite basis representation, although the implementation can be tedious. The solution of the corresponding Schrödinger equation can be obtained in either a time-independent[29,42] or time-dependent fashion,[26] but the latter initial value problem is typically easier to handle. The major numerical obstacle in geometric phase corrected quantum dynamics is how to treat singularities in both the closely related derivative coupling and DBOC near the conical intersection.

D. An MAB topography

As observed in the past,[65] a saddle point can be viewed as derived from the lower cone of a conical intersection with the introduction of quadratic terms into the Hamiltonian. This

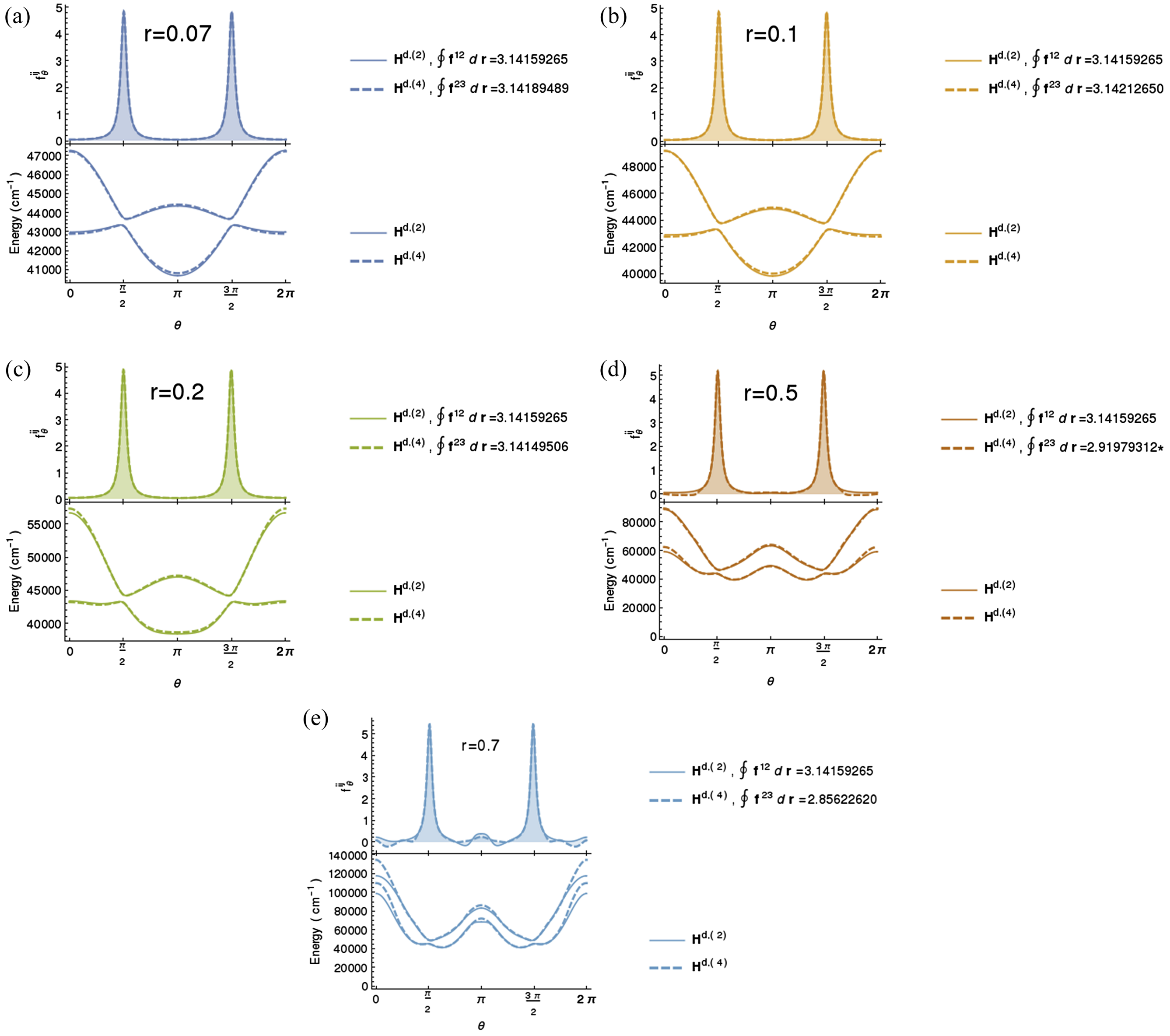

FIG. 3. $\mathbf{f}^{(a),mx,S_1,S_2}(\mathbf{R})$ and circulations (upper panel), and S$_1$ and S$_2$ energies (lower panel). Solid lines $\mathbf{H}^{d,(2)}$, dashed lines $\mathbf{H}^{d,(4)}$ determined quantities. Demonstration that the two-state diabatization is removable, has zero curl, and has the θ dependence exhibited in Eq. (11a), independent of r. The 4 state diabatization is seen to have a nonremovable part which deviates significantly from Eq. (11a) result for large displacements. For reference π = 3.141 592 65. * indicates double-valued $\mathbf{f}^{(a),m4,S_1,S_2}(\mathbf{R})$.

connection between a conical intersection and low energy saddle points shows how low energy paths around conical intersections may come to exist. Thus the MAB effect inducing topography presented in Fig. 1 is not likely to be rare. This observation and the above mathematical analysis show that the MAB effect is a two-state description of geometric phase issues. In a qualitative sense the lower potential energy surface governs the dynamics while the upper state gives rise to the geometric phase effect. Thus it is not surprising that a general analysis of the MAB effect requires knowledge of the interaction between two states (Eq. (17)) provided by the derivative coupling.

It is possible to imagine more complex topographies where motion is restricted to the lowest potential energy surface and intersections of states 1 and 2, as well as intersections of states 2 and 3 must be considered. While a general analysis of this situation is reserved for future work, its relevance in the present context[66] will be discussed below.

III. NUMERICAL EXAMPLES

In this section, we address the practical issues encountered in using Eq. (13a) to include the geometric phase in dynamics on a single potential energy surface. The example we use is phenol photodissociation through its excited S_1 state, $C_6H_5OH(S_0) + h\nu \rightarrow C_6H_5OH(S_1,S_2) \rightarrow C_6H_5O + H$, which has been the subject of much recent interest.[65,67–78] As seen in Fig. 1, there is a low-lying S_1-S_2 conical intersection and two, symmetrically displaced, lower-energy adiabatic saddle points on S_1. This topography can give rise to the MAB effect for adiabatic dissociative dynamics on S_1.[15] The system will be treated here in its full $3N^{atom} = 39$-dimensions.

Two directly comparable coupled diabatic state representations, described in more detail in the Appendix, are employed: a shifted[79] 4 diabatic state (S_0, S_1, S_2, S_3) representation, $\mathbf{H}^{d,(4)}$, previously reported[79] and a shifted two diabatic state (S_1, S_2) representation $\mathbf{H}^{d,(2)}$. Thus, S_1 and S_2 are states 1 and 2 from $\mathbf{H}^{d,(2)}$ while they are states 2 and 3 from $\mathbf{H}^{d,(4)}$. It should be emphasized that $\mathbf{H}^{d,(2)}$ is designed to treat the S_1-S_2 conical intersection only while $\mathbf{H}^{d,(4)}$ is more generally applicable. However both coupled diabatic state representations are suitable for describing phenol photodissociation. Here the principal issue is that the $\mathbf{f}^{(a),(m4),S_1,S_2}$ obtained from $\mathbf{H}^{d,(4)}$ are nonremovable while $\mathbf{f}^{(a),(m2),S_1,S_2}$ obtained from $\mathbf{H}^{d,(2)}$ are removable. Table I compares $\mathbf{H}^{d,(m)}$ $m = 2,4$ determined energies at key geometries: the S_1 minimum [min(S_1)], the S_1 transition state [ts(S_1)], and the S_1-S_2 minimum energy crossing [mex(S_1-S_2)] together with g and h. The agreement is seen to be good.

The $\mathbf{H}^{d,(2)}$ determined S_1 adiabatic energies and the $\mathbf{f}^{(a),(m2),S_1,S_2}(\mathbf{R})$ constitute the input needed to construct H^{MAB} in Eq. (17). In this section we assess the numerical accuracy of this approach. We note that the overall sign of the reported circulations depends on the sign of the initial $\mathbf{f}^{(a),(m2),S_1,S_2}(\mathbf{R})$. Since this sign is irrelevant in the present context, we only use it to improve the clarity of the figures that follow. Our tripartite analysis will consider the following points: (i) we will determine the size and kind of error in the circulations attributable to the nonremovable derivative couplings, $\mathbf{f}^{(a),(m4),S_1,S_2}(\mathbf{R})$; (ii) although the results of Section II show that the circulations of the removable derivative couplings $\mathbf{f}^{(a),(m2),S_1,S_2}(\mathbf{R})$ will be multiples (including 0) of π, it is important to consider the accuracy of the numerical quadratures and how the numerical errors compare to the errors attributable to nonremovability; and (iii) we will demonstrate that seam curvature, which is omitted in simplified models of the MAB effect, is well described by the present approach.

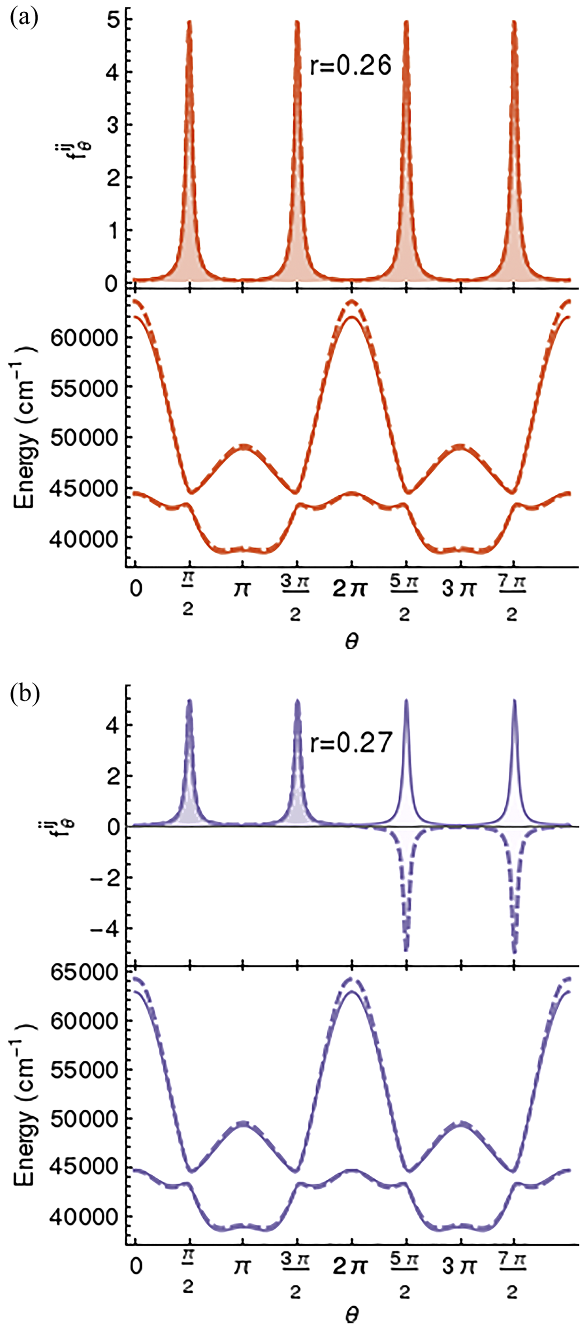

FIG. 4. Single-valued (a) $r = 0.26$ vs double-valued (b) $r = 0.27$ $\mathbf{f}^{(a),m4,S_1,S_2}(\mathbf{R})$. Also shown are $\mathbf{f}^{(a),m2,S_1,S_2}(\mathbf{R})$ which is always single-valued. Lower part of each panel reports the energies of states S_1 and S_2. Solid lines $\mathbf{H}^{d,(2)}$, dashed lines $\mathbf{H}^{d,(4)}$ determined quantities.

A. Orthogonal intersection adapted coordinates

To properly compare the $\mathbf{H}^{d,(4)}$ and $\mathbf{H}^{d,(2)}$ determined results, they will be presented in individual orthogonal intersection adapted coordinate systems using cylindrical polar coordinates, as defined following Eq. (8c). Table I reports the magnitudes of the $\boldsymbol{g}$ and $\boldsymbol{h}$ vectors used to construct the coordinate system. Their good agreement reflects the fact that $\mathbf{H}^{d,(2)}$ provides a removable approximation to the adiabatic representation associated with $\mathbf{H}^{d,(4)}$.

B. Origin centered loops

Figures 2–4 illustrate the evaluation of

$$C(w,\mathbf{O},r) = \oint \mathbf{f}^{(a),(mw),S_2,S_1}(\mathbf{R}')\cdot d\mathbf{R}', \qquad (18)$$

the circulation of the $\mathbf{H}^{d,(w)}$ ($w = 2,4$) determined derivative coupling $\mathbf{f}^{(a),(mw),S_1,S_2}(\mathbf{R})$ along circles in the g-h plane centered at $\mathbf{O} = (x^0, y^0, \mathbf{z}^0) = (0,0,\mathbf{0})$ with radii $\rho = r = (0.07, 0.1, 0.2, 0.26, 0.27, 0.5,$ and $0.7)$ pictured in Fig. 2. Figs. 3(a) – 3(f) juxtapose the $\mathbf{H}^{d,(2)}$ and $\mathbf{H}^{d,(4)}$ determined energies and derivative couplings at the indicated r. The circulations are tabulated in Table II. For $C(2,(0,0,\mathbf{0}), r \le 0.7)$ the integral consists of two identical halves which add to give π exact to 8 decimal places regardless of the radius r. This indicates the quality of $f_\theta^{(a),(m2),S_1,S_2}(\rho,\theta)$ and that a single conical intersection (at the origin) is enclosed in the loop. The peaks in $f_\theta^{(a),(m2),S_1,S_2}(\rho,\theta)$ at $\theta = \pi/2$ and $3\pi/2$, evident in Figs. 3(a)–3(e), arise from Eq. (11a) reflecting the ratio g/h (~10) in Table I. The accuracy of these circulations strongly supports the utility of this approach. Note the good agreement between the $\mathbf{H}^{d,(4)}$ and $\mathbf{H}^{d,(2)}$ determined energies in Figs. 3(a)–3(e).

For $C(4,(0,0,\mathbf{0}), r \le 0.2)$, the contribution of the nonremovable part of $f_\theta^{(a),(m4),S_1,S_2}(\rho,\theta)$ is quite small and although increasing with increasing r, it probably could be tolerated in numerical calculations. Even for $0.2 < r \le 0.27$ a.u. the circulation is not that far from π. The increase in the nonremovable contribution with increasing r reflects an increase in the derivative coupling of states 3 and 4 as their separation decreases. When states 3 and 4 intersect conically, the situation changes abruptly and dramatically. This situation is evinced in Figs. 4(a) and 4(b), which describe that $r = 0.26$ a.u. and $r = 0.27$ a.u., respectively. The results are completely consistent with the formal analysis of linked conical intersections in Ref. 66 denoted as *HY* below. For $\mathbf{H}^{d,(4)}$, the loop already includes a 2-3 conical intersection at the origin. The existence of a 3-4 conical intersection in the loop, which occurs for 0.26 a.u $< r \le 0.27$ a.u., renders $\mathbf{f}^{(a),m4,2,3}(\rho = 0.27,\theta)$ double-valued, since now state 3 does not change sign on traversing the loop but state 2 does. In the latter case, conical intersections of states 2 and 3 and 3 and 4 are referred to as linked intersections by *HY*. *HY* show that for linked conical intersections of states I, J, K, the I, J circulation depends on the starting point! Further the circulation from 0 to 4π is zero rather than twice the integral from 0 to 2π as would be expected. Compare Figs. 4(a) and 4(b). $r = 0.27$ a.u. is the beginning of a complete disaster for using $\mathbf{H}^{d,(4)}$ to construct the requisite circulation although it is not evident from the (starting point dependent) value of the circulation. This situation holds for $0.27 \le r < 0.6$ a.u.,

TABLE II. Circulations $C(w,(0,0,\mathbf{0}),r)$. Effect of the nonremovable part.

r	$w = 2$	$w = 4$
0.07	3.141 592 65	3.141 894 89
0.1	3.141 592 65	3.142 126 50
0.2	3.141 592 65	3.141 950 62
0.26	3.141 592 65	3.131 307 72
0.27	3.141 592 65	3.106 175 36[a]
0.3	3.141 592 65	3.064 390 78[a]
0.4	3.141 592 65	2.973 488 40[a]
0.5	3.141 592 65	2.919 793 12[a]
0.6	3.141 592 65	2.856 226 21[a]
0.7	3.141 592 65	2.856 226 21

[a] Double-valued $\mathbf{f}^{(a),m4,S_1,S_2}$.

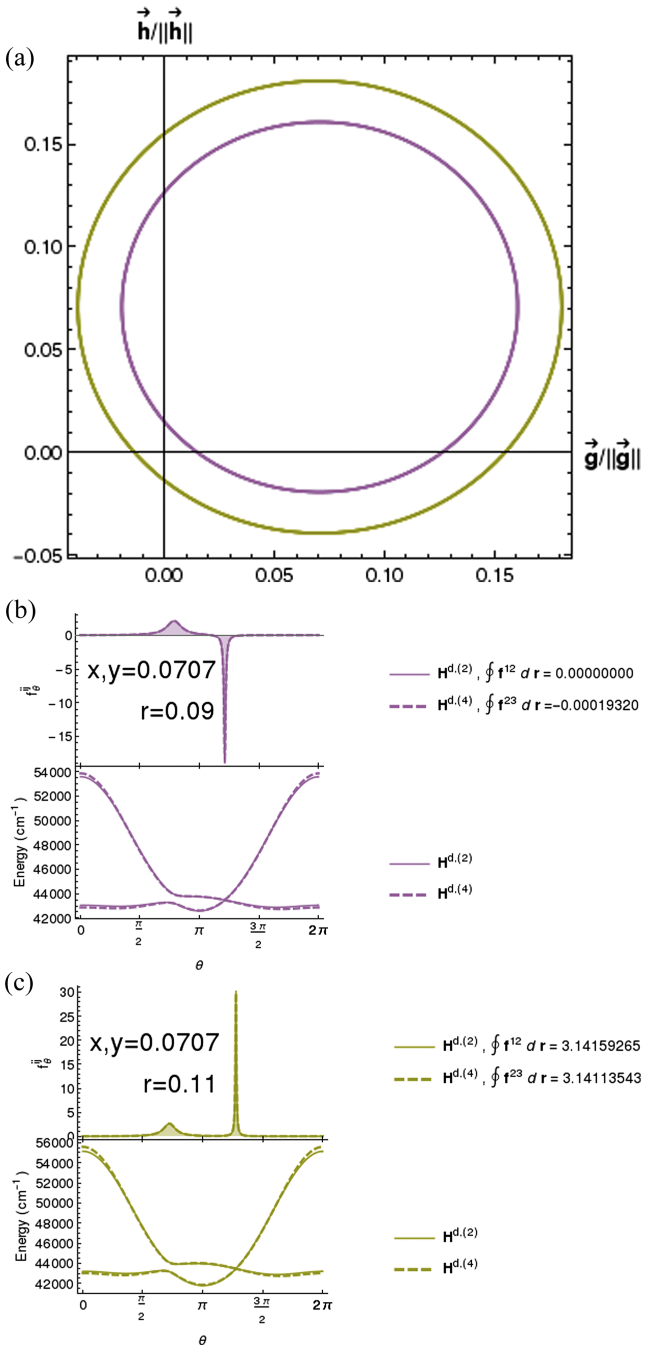

FIG. 5. Demonstration that if no[blue] (one[green]) conical intersection is contained anywhere in the loop presented in panel (a) the circulation gives $0(\pi)$ as required. The 4 state diabatization is seen to have a small nonremovable part. Panels (b) and (c) report circulations, $\mathbf{f}^{(a),mx,S_1,S_2}(\mathbf{R})$ and the energies of states S_1 and S_2, respectively. Solid lines $\mathbf{H}^{d,(2)}$, dashed lines $\mathbf{H}^{d,(4)}$ determined quantities.

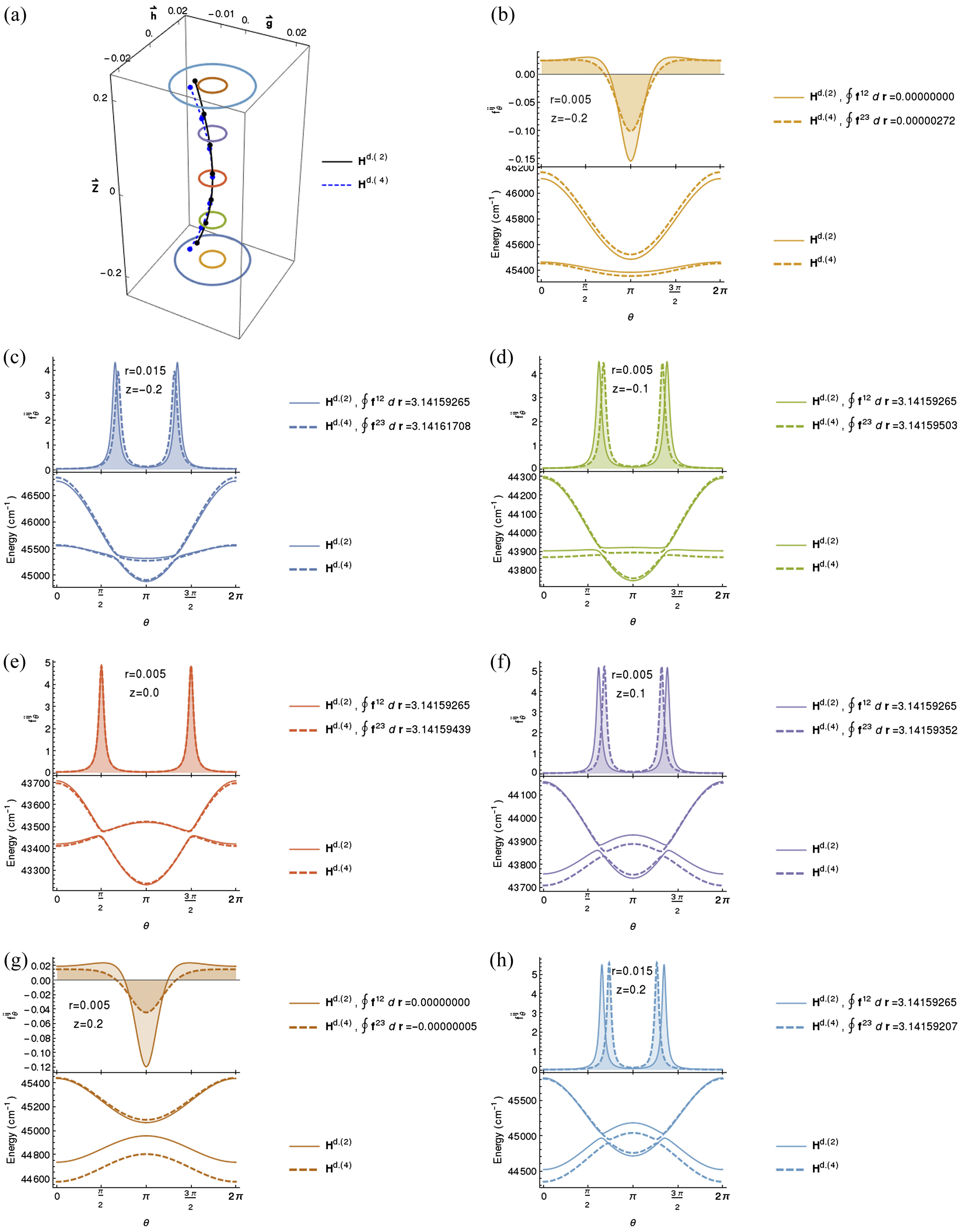

FIG. 6. Seam curvature. Loops in the g-h plane displaced along a z_i-axis demonstrating the effect of seam curvature along the z_i direction on the circulation.

although beyond $r = 0.3$ a.u., energy considerations limit the importance of circular paths. It is worth noting that for 0.6 a.u. $< r \leq 0.7$ a.u., a second 3-4 intersection is present in the loop and $\mathbf{f}^{(a),m4,2,3}(\rho, \theta)$ is again single-valued. As is evident from Table II, this pathology does not occur for $\mathbf{H}^{d,(2)}$ which has only two states.

C. Displaced conical intersections

With the frequently used linear vibronic coupling model,[80] there is only a single conical intersection in the g-h plane which is usually taken as the origin. However, when quadratic terms are included, additional seams of conical intersections can exist which intersect the g-h

plane.[81,82] Consequently, it is relevant to consider conical intersections which do not occur at the center of a circle. This can give rise to the type of circulation illustrated in Figs. 5(b) and 5(c) which consider $\mathbf{H}^{d,(2)}$ and $\mathbf{H}^{d,(4)}$ determined circulations for loops pictured in Fig. 5(a). In these figures the origin is not a conical intersection. Thus, for $w = 2$ the circulation $C(w,(t^s,t^s,\mathbf{0}),r) = 0$ for $r < t^s\sqrt{2}$ (Fig. 5(b)) and $\mathrm{C}(w,(t^s,t^s,\mathbf{0}),r) = \pi$ for $r > t^s\sqrt{2}$ (Fig. 5(c)). For $w = 4$ a small nonremovable part is evinced.

D. Seam curvature

Up to this point we have considered a single point of conical intersection. Our final example considers the effect of seam curvature and how the line integral correctly accounts for it. Seam curvature, the fact that for $\mathbf{z} \neq 0$ conical intersections do not occur at $(x,y) = (0,0)$, is illustrated in Fig. 6(a) which shows the $\mathbf{H}^{d,(2)}$ and $\mathbf{H}^{d,(4)}$ determined seams. The rectangular parallelepiped shows the seam (black line) determined as a function of R(CO), as a function of (x,y,z_2). Loops are constructed for fixed values of $\mathbf{z}$ in a plane parallel to the g-h plane. The loops used to evaluate circulations $C(w,(0,0,\mathrm{z}_2),r)$ are shown in the parallelepiped. Corresponding circulations and plots of $f_\theta^{(a),mw,S_2,S_1}(r,\theta)$ are given to the right. Near $\mathbf{z} = 0$ $C(w,(0,0,\mathrm{z}_2),r) = \pi$ for all r as the conical intersection at $(x,y,\mathbf{z})$ is close to $(0,0,\mathbf{z})$. However, as seen from Figs. 6(b)–6(h), as $|\mathbf{z}|$ increases the $\rho_c = (x^2 + y^2)^{1/2}$ for the conical intersection increases so that for $r < \rho_c$ $C(w,(0,0,z_2),r) = 0$ since no conical intersection is contained in the loop. Increasing r eventually encloses the conical intersection and $C(w,(0,0,\mathrm{z}_2),r)$ becomes π. Here it is important to note that the only computed values of $C(2,(0,0,\mathrm{z}_2),r)$ are 0 or π. This essential aspect of the MAB effect is ignored in the linear vibronic coupling model of conical intersections. Similar results are obtained for $w = 4$, indicating that the nonremovable contribution is small.

IV. SUMMARY AND CONCLUSIONS

The MAB effect is the effect that energy inaccessible conical intersections have on adiabatic single state dynamics through the geometric phase. Recently there has been considerable theoretical work on tunneling in phenol.[15,65,72,77,78] Of particular relevance here are studies of nonadiabatic tunneling which suggest that including the MAB effect can change the predicted tunneling dissociation rate by over an order of magnitude.[15,16] There has been limited consideration of the MAB effect on classically allowed or tunneling reaction dynamics owing to technical issues: the lack of a computationally useful general formulation of the MAB Hamiltonian and a method of dealing with the singular terms in the MAB Hamiltonian. Neither the prevalence nor magnitude of the MAB effect is well-characterized. Since in principle the possibility of an MAB effect must be considered in all adiabatic treatments of nuclear dynamics especially for excited electronic states, the effect is potentially transformative.

The methodology proposed here eliminates the first hurdle, which is the *ab initio* determination of the phase factor used to render the total wavefunction single-valued. In future work we will consider the numerical issues associated with solving Eq. (17), address the prevalence of the MAB effect in the nuclear dynamics, particularly when $\psi_I^{(a)}(\mathbf{q};\ \mathbf{R})$ is an excited electronic state, and describe the topographical factors that determine the size of the effect.

Note that in principle it is possible to avoid the inclusion of the MAB effect provided the dynamics is treated in the two diabatic state approximation. However, given the increase in computational complexity in processing two diabatic states compared one adiabatic state, it is best to avoid this situation when possible. In addition, the diabatic representation, which is only determined up to a geometry independent orthogonal transformation, does not succinctly capture the physics of the more concise adiabatic representation. The approach espoused here is best suited for fitted surfaces. It fails, perhaps catastrophically, when *ab initio* data are used directly. However the use of fit surfaces should not be viewed as a (significant) limitation since fit surfaces are preferred for detailed quantum dynamics calculations and as discussed in detail in Ref. 43 are actually better representations of the coupled PESs than the *ab initio* data from which they are derived.

SUPPLEMENTARY MATERIAL

See supplementary material for the fit surfaces $\mathbf{H}^{d,(2)}$ and $\mathbf{H}^{d,(4)}$ used in this work. Our submission is supplemented with two .tar files (for $\mathbf{H}^{d,(2)}$ and $\mathbf{H}^{d,(4)}$) which contain the requisite MAKE, FORTRAN, and INPUT files for the evaluation of the adiabatic energy, energy gradient, derivative coupling, and diabatic energies and couplings at an arbitrary point. Sample OUTPUTs are provided as README files. The $\mathbf{H}^{d,w}$ used in this work are also available online. For $w = 4$, $\mathbf{H}^{d,(4)}$ is available at https://www.github.com/yarkonygrp/surfaces/phenol/4state and for $w = 2$, at https://www.github.com/yarkonygrp/surfaces/phenol/2state.

ACKNOWLEDGMENTS

D.R.Y. acknowledges the support of NSF Grant No. CHE-1361121. H.G. thanks the Department of Energy for support (Grant No. DE-SC0015997).

APPENDIX: $\mathbf{H}^d$

The $\mathbf{H}^{d,(\mathrm{n})}$ employed in this work have the form[79]

$$ {}^s\mathbf{H}^d(\mathbf{R}) = \mathbf{H}^d(\mathbf{R}) + \sum_{j=1}^{N^{state}} V_j^s \mathbf{B}^{j,j}, \tag{A1a} $$

where

$$ \mathbf{H}^d(\mathbf{R}) = \sum_{l=1}^{N^c} V_l[\hat{P}^{Ir[u(l)],Ir[v(l)]} g^{(l)}(\mathbf{R})]\mathbf{B}^{u(l),v(l)}, \tag{A1b} $$

$\mathbf{B}^{u,v}$ is an $N^{state} \times N^{state}$ symmetric matrix with a 1 in (u,v) and (v,u) elements and the remaining elements are 0. $\hat{P}^\kappa$ is a projection operator for the κ^{th} irreducible representation (Ir) of the appropriate complete nuclear permutation inversion (CNPI)[83] subgroup, here G_4. The $g^{(l)}$ are products of functions of the $\mathbf{r}_{i,j} = \mathbf{R}_i - \mathbf{R}_j$ and $r_{i,j} = |\mathbf{r}_{i,j}|$ for $1 \leq i < j \leq N^{atom}$. A complete description of the $g^{(l)}$ is found in Ref. 74. The V_l are

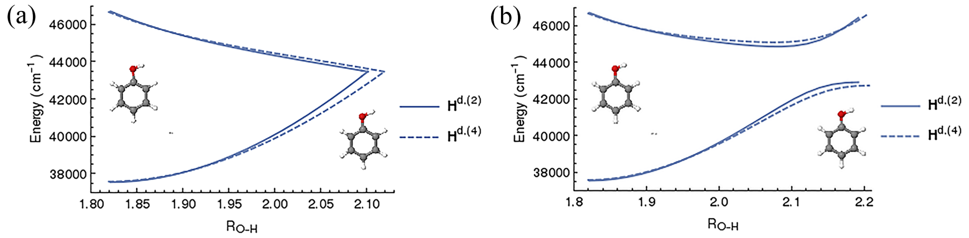

FIG. 7. Plot of $\mathbf{H}^{d,(4)}$ (dashed lines) and $\mathbf{H}^{d,(2)}$ (solid lines) determined energy along linear synchronous transit path from: plate (a)_min(S_1) – mex(S_1 -S_2) and plate (b)_min(S_1) –ts(S_1).

the N^c linear coefficients of combination determined by the fitting procedure.[74] As formulated in Ref. 79 $\mathbf{H}^d$ is obtained by fitting the *ab initio* data energies, energy gradients, and derivative couplings, while the V_i^s are empirical geometry independent shifts designed to improve the calculated spectrum of ${}^s\mathbf{H}^d$ when compared with very accurate computational results or experiment.

In this work, $\mathbf{H}^{d,(4)}$ is the $\mathbf{H}^d$ reported in Ref. 74, shifted for reasons described in Ref. 79 by $V^s_{^1B_2} = -1800\ \text{cm}^{-1}$ and $V^s_{^1B_1} = -1038\ \text{cm}^{-1}$. $\mathbf{H}^{d,(2)}$ is constructed from an intermediate $\mathbf{H}^{d,int}$ determined from ${}^s\mathbf{H}^d$ computed energies, energy gradients, and derivative couplings evaluated at a total of 2335 points. ${}^s\mathbf{H}^d$ is the above $\mathbf{H}^d$ shifted by $V^s_{^1B_2} = -1800\ \text{cm}^{-1}$. The $\mathbf{H}^{d,int}$ expansion is comprised of $N^c = 5145$ coefficients, defined by 140 443 equations satisfied in a least squares sense. The mean unsigned (root mean square) error for the energy is 39.73 (92.95) cm^{-1} and that for the energy gradient is 4.82(6.19)%. This fit was determined for R(O–H) <1.8 Å, the region for which single state S_1 dynamics will be considered. $\mathbf{H}^{d,(2)}$ is then $\mathbf{H}^{d,int}$ shifted by $V^s_{^1B_1} = -1008.0\ \text{cm}^{-1}$ and can be directly compared with $\mathbf{H}^{d,(4)}$. Comparisons of the $\mathbf{H}^{d,(2)}$ and $\mathbf{H}^{d,(4)}$ determined S_1 energies along paths from min(S_1) to ts(S_1) and from min(S_1) to mex(S_1-S_2) are reported in Figs. 7(a) and 7(b), respectively. Additional comparisons are provided in Table I and Figs. 3–6.

[1] E. Teller, J. Phys. Chem. **41**, 109 (1937).
[2] A. Migani and M. Olivucci, in *Conical Intersections: Electronic Structure, Dynamics and Spectroscopy*, edited by W. Domcke, D. R. Yarkony, and H. Köppel (World Scientific, Singapore, 2004), p. 271.
[3] M. J. Paterson, M. J. Bearpark, M. A. Robb, L. Blancafort, and G. A. Worth, Phys. Chem. Chem. Phys. **7**, 2100 (2005).
[4] B. G. Levine and T. J. Martínez, Annu. Rev. Phys. Chem. **58**, 613 (2007).
[5] S. Matsika and P. Krause, Annu. Rev. Phys. Chem. **62**, 621 (2011).
[6] W. Domcke and D. R. Yarkony, Annu. Rev. Phys. Chem. **63**, 325 (2012).
[7] X. Zhu and D. R. Yarkony, Mol. Phys. **13**, 1983 (2016).
[8] G. Herzberg and H. C. Longuet-Higgins, Discuss. Faraday Soc. **35**, 77 (1963).
[9] H. C. Longuet-Higgins, Adv. Spectrosc. **2**, 429 (1961).
[10] C. A. Mead and D. G. Truhlar, J. Chem. Phys. **70**, 2284 (1979).
[11] M. V. Berry, Proc. R. Soc. A **392**, 45 (1984).
[12] I. Bersuker, *The Jahn-Teller Effect* (Cambridge University Press, Cambridge, 2006).
[13] T. C. Thompson, G. Izmirlian, S. J. Lemon, D. G. Truhlar, and C. A. Mead, J. Chem. Phys. **82**, 5597 (1985).
[14] C. A. Mead, Chem. Phys. **49**, 23 (1980).
[15] C. Xie, J. Ma, X. Zhu, D. R. Yarkony, D. Xie, and H. Guo, J. Am. Chem. Soc. **138**, 7828 (2016).
[16] C. Xie, D. R. Yarkony, and H. Guo, "Nonadiabatic tunneling via conical intersections and the role of the geometric phase," Phys. Rev. Lett. (submitted).
[17] C. A. Mead, J. Chem. Phys. **72**, 3839 (1980).
[18] S. C. Althorpe, J. Chem. Phys. **124**, 084105 (2006).
[19] A. J. C. Varandas, F. B. Brown, C. A. Mead, D. G. Truhlar, and N. C. Blais, J. Chem. Phys. **86**, 6258 (1987).
[20] A. Kuppermann, in *Dynamics of Molecules and Chemical Reactions*, edited by R. E. Wyatt and J. Z. H. Zhang (Marcel Dekker, Inc., New York, 1996), p. 411.
[21] A. Kuppermann and Y.-S. M. Wu, Chem. Phys. Lett. **205**, 577 (1993).
[22] B. Lepetit, Z. Peng, and A. Kuppermann, Chem. Phys. Lett. **166**, 572 (1990).
[23] Y.-S. M. Wu and A. Kuppermann, Chem. Phys. Lett. **201**, 178 (1993).
[24] Y.-S. M. Wu and A. Kuppermann, Chem. Phys. Lett. **235**, 105 (1995).
[25] B. K. Kendrick, J. Phys. Chem. A **107**, 6739 (2003).
[26] J. C. Juanes-Marcos and S. C. Althorpe, J. Chem. Phys. **122**, 204324 (2005).
[27] S. Mahapatra, H. Köppel, and L. Cederbaum, J. Phys. Chem. A **105**, 2321 (2001).
[28] F. Bouakline, S. C. Althorpe, and D. Peláez Ruiz, J. Chem. Phys. **128**, 124322 (2008).
[29] B. K. Kendrick, J. Chem. Phys. **112**, 5679 (2000).
[30] J. Jankunas, M. Sneha, R. N. Zare, F. Bouakline, and S. C. Althorpe, J. Chem. Phys. **139**, 144316 (2013).
[31] B. K. Kendrick, J. Hazra, and N. Balakrishnan, Phys. Rev. Lett. **115**, 153201 (2015).
[32] B. K. Kendrick, J. Hazra, and N. Balakrishnan, J. Chem. Phys. **145**, 164303 (2016).
[33] H. Guo and D. R. Yarkony, Phys. Chem. Chem. Phys. **18**, 26335 (2016).
[34] I. G. Ryabinkin and A. F. Izmaylov, Phys. Rev. Lett. **111**, 220406 (2013).
[35] R. Gherib, I. Ryabinkin, and A. F. Izmaylov, J. Chem. Theory Comput. **11**, 1375 (2015).
[36] R. Gherib, L. Ye, I. G. Ryabinkin, and A. F. Izmaylov, J. Chem. Phys. **144**, 154103 (2016).
[37] A. F. Izmaylov, J. Chem. Phys. **138**, 104115 (2013).
[38] L. Joubert-Doriol, I. G. Ryabinkin, and A. F. Izmaylov, J. Chem. Phys. **139**, 234103 (2013).
[39] I. G. Ryabinkin, L. Joubert-Doriol, and A. F. Izmaylov, J. Chem. Phys. **140**, 214116 (2014).
[40] S. C. Althorpe, T. Stecher, and F. Bouakline, J. Chem. Phys. **129**, 214117 (2008).
[41] J. C. Juanes-Marcos, S. C. Althorpe, and E. Wrede, Science **309**, 1227 (2005).
[42] B. Kendrick and R. T. Pack, J. Chem. Phys. **104**, 7502 (1996).
[43] X. Zhu and D. R. Yarkony, J. Chem. Phys. **140**, 024112 (2014).
[44] W. Kolos and L. Wolniewlcz, J. Chem. Phys. **41**, 3663 (1964).
[45] L. I. Kleinman and M. Wolfsberg, J. Chem. Phys. **60**, 4749 (1974).
[46] B. C. Garrett and D. G. Truhlar, J. Chem. Phys **82**, 4543 (1985).
[47] J. O. Jensen and D. R. Yarkony, J. Chem. Phys. **89**, 975 (1988).
[48] N. C. Handy, Y. Yamaguchi, and H. F. Schaefer, J. Chem. Phys. **84**, 4481 (1986).
[49] E. F. Valeev and C. D. Sherrill, J. Chem. Phys. **118**, 3921 (2003).
[50] D. R. Yarkony, J. Phys. Chem. A **101**, 4263 (1997).
[51] D. R. Yarkony, J. Chem. Phys. **112**, 2111 (2000).
[52] C. A. Mead and D. G. Truhlar, J. Chem. Phys. **77**, 6090 (1982).
[53] M. Baer, Chem. Phys. **15**, 49 (1976).
[54] X. Zhu and D. R. Yarkony, J. Phys. Chem. A **119**, 12383 (2015).
[55] X. Zhu and D. R. Yarkony, J. Chem. Phys. **144**, 044104 (2016).
[56] M. Baer, J. Phys. Chem. A **104**, 3181 (2000).
[57] M. Baer, *Beyond Born-Oppenheimer* (John Wiley and Sons, Hoboken, 2006).
[58] R. Baer, J. Chem. Phys. **117**, 7405 (2002).
[59] T. Pacher, C. A. Mead, L. S. Cederbaum, and H. Köppel, J. Chem. Phys. **91**, 7057 (1989).
[60] D. R. Yarkony, J. Chem. Phys. **114**, 2601 (2001).
[61] B. K. Kendrick, C. A. Mead, and D. G. Truhlar, J. Chem. Phys. **107**, 7594 (1999).
[62] C. A. Mead, J. Chem. Phys. **78**, 807 (1983).
[63] A. J. C. Varandas and Z. R. Xu, Chem. Phys. Lett. **316**, 248 (2000).

[64] B. Kendrick, C. A. Mead, and D. G. Truhlar, Chem. Phys. Lett. **330**, 629 (2000).
[65] X. Xu, J. J. Zheng, K. R. Yang, and D. G. Truhlar, J. Am. Chem. Soc. **136**, 16378 (2014).
[66] S. Han and D. R. Yarkony, J. Chem. Phys. **119**, 5058 (2003).
[67] M. Abe, Y. Ohtsuki, Y. Fujimura, and W. Domcke, J. Chem. Phys. **123**, 064313 (2005).
[68] H. An and K. Baeck, J. Phys. Chem. A **115**, 13309 (2011).
[69] M. N. R. Ashfold, A. L. Devine, R. N. Dixon, G. A. King, M. G. D. Nix, and T. A. A. Oliver, Proc. Natl. Acad. Sci. U. S. A. **105**, 12701 (2008).
[70] H. D. Bist, J. C. D. Brand, and D. R. Williams, J. Mol. Spectrosc. **21**, 76 (1966).
[71] H. D. Bist, J. C. D. Brand, and D. R. Williams, J. Mol. Spectrosc. **24**, 413 (1967).
[72] R. N. Dixon, T. A. A. Oliver, and M. N. R. Ashfold, J. Chem. Phys. **134**, 194303 (2011).
[73] M. L. Hause, Y. H. Yoon, A. S. Case, and F. F. Crim, J. Chem. Phys. **128**, 104307 (2008).
[74] X. Zhu and D. R. Yarkony, J. Chem. Phys. **144**, 024105 (2016).
[75] A. L. Sobolewski and W. Domcke, J. Phys. Chem. A **105**, 9275 (2001).
[76] Z. Lan, W. Domcke, V. Vallet, A. L. Sobolewski, and S. Mahapatra, J. Chem. Phys. **122**, 224315 (2005).
[77] X. Xu, K. R. Yang, and D. G. Truhlar, J. Chem. Theory Comput. **9**, 3612 (2013).
[78] K. R. Yang, X. Xu, J. Zheng, and D. G. Truhlar, Chem. Sci. **5**, 4661 (2014).
[79] X. Zhu, C. L. Malbon, and D. R. Yarkony, J. Chem. Phys. **144**, 124312 (2016).
[80] H. Köppel, W. Domcke, and L. S. Cederbaum, in *Conical Intersections*, edited by W. Domcke, D. R. Yarkony, and H. Köppel (World Scientific, New Jersey, 2004), p. 323.
[81] J. W. Zwanziger and E. R. Grant, J. Chem. Phys. **87**, 2954 (1987).
[82] M. Schuurman and D. R. Yarkony, J. Chem. Phys. **126**, 044104 (2007).
[83] P. R. Bunker and P. Jensen, *Molecular Symmetry and Spectroscopy*, 2nd ed. (NRC Research Press, Ottawa, 1998).